Modelling the Genesis of Sand-Starved Dunes in Steady Currents

Gaetano Porcile [1], Johan H. Damveld [2], Pieter C. Roos [2], Paolo Blondeaux [3], Marco Colombini [3]

[1] **Coastal and Continental Morphodynamics Laboratory, University of Normandy, 24 rue des Tilleuls, 14000 Caen, France**

[2] **Water Engineering and Management, University of Twente, PO Box 217, 7500 AE Enschede, the Netherlands**

[3] **Department of Civil, Chemical and Environmental Engineering, University of Genoa, 16145, Via Montallegro 1 Genoa, Italy**

Abstract

The formation of fluvial dunes has been usually investigated assuming an infinite availability of the mobile sediment. Field observations and laboratory experiments nevertheless indicate that the volume of sediment available for transport affects their morphology. Here we undertake a stability analysis showing the formation of sand dunes in steady currents accounting for the effects of sediment starvation on their formative mechanisms and compare it against laboratory experiments and an application of a fully numerical commercial model of finite amplitude dunes, thus enabling an improved understanding of the genesis of starved fluvial dunes. Both small and finite amplitude dunes are shown to be affected by sediment starvation. As their growth progressively exposes a motionless substratum, both models predict the lengthening of starved dunes with increasing irregularity in their spacing. These findings conform with the outcome of physical experiments performed earlier in a laboratory flume and existing measurements of starved fluvial dunes in the field.

Plain Language Summary

The formation of fluvial dunes has been usually investigated assuming an infinite availability of the sediment that can be entrained by the streaming flow. Field observations and laboratory experiments nevertheless indicate that the volume of sediment available for transport affects their morphology. Here we present a theoretical model of the formation of small amplitude sand dunes in steady currents accounting for the effects that the lack of sediment has on their formative mechanisms and compare it against laboratory experiments and an application of a numerical commercial model, thus enabling an improved understanding of the genesis of fluvial dunes in sediment starved environments. Both models predict similar characteristics of starved dunes, describing their lengthening with increasing irregularity in their spacing as their growth progressively exposes a motionless substratum. These findings agree with the results of laboratory experiments and existing measurements of starved fluvial dunes in the field.

1 Introduction

River beds are seldom flat and those that contain sand generally exhibit a fascinating variety of bedforms, ranging from small-scale transverse ripples to large-scale longitudinal bars (Allen, 1968). Whenever the shear induced by water flowing over granular surfaces exceeds its threshold value for sediment motion, sediment particles begin to move and then sediment patterns might appear as a result of instability of the erodible river bed (Seminara, 2010). The flow of water and sediment produce these bedforms, which, in turn, profoundly influence water levels and sediment transport locally affecting mass and momentum transfer. In particular, transverse bedforms typically grow perpendicular to the main direction of the river stream and thus their presence is a primary source of flow roughness and a major factor in determining water levels (Engelund and Fredsoe, 1982). For practical purposes, the effect that these bedforms have on the hydrodynamics can be modelled as a hydraulic roughness of appropriate size. As such, unravelling the processes underlying their morphology is a subject of great concern to river engineering.

Fluvial dunes are one dimensional bedforms periodic in the longitudinal direction. They exhibit asymmetric profiles with fairly regular crests migrating invariably down-stream (Guy et al., 1966). Their typical crest-to-crest distances scale with the local water depth and their appearance is associated with subcritical flows in the Froude sense (Colombini, 2004). Because of their significance in formulating depth-discharge relations for river flows and predictor formulae for sediment transport, fluvial dunes received extensive attention from engineers and geomorphologists.

Many field observations and laboratory measurements indicate that sediment patterns commonly observed where large amounts of mobile sediment are available, i.e., alluvial bedforms, differ from those formed where mobile sediment is scarce, i.e., starved bedforms. Hereinafter we will refer to the latter conditions as sediment starvation. In fluvial environments sediment starvation is common. As channel slopes decrease, rivers typically exhibit abrupt transitions from gravel to sandy bottoms. In these transitional settings, seasonal and perennial streams subject to periods of low flow or discharge waves undergo a transient degradation until they are fully armoured (Parker et al., 1982). Then the natural formation of such armoured layer inhibits the entrainment of finer sediment from the bed, eventually resulting in sediment starvation. Whereby the armoured bed is developed and finer material continues to be supplied to the water flow, starved dunes may appear.

Recent advances in the physical modelling of fluvial starved bedforms revealed the effects of sediment starvation on bedform development. By means of a very simple phenomenological experiment, Venditti et al. (2017) described a definable sequence of starved bedforms emerging in steady currents depending on the supply of sediment. As the sediment supply from upstream increases, a gradual transition occurs starting from longitudinal sand ribbons to three-dimensional barchans that eventually coalesce onto amorphous sandy mounds ultimately leading to the generation of two-dimensional trasverse dunes (Kleinhans et al., 2002). However, still unclear is

how the lack of sediment affects the morphology of the resultant starved dunes. Only a few observations are available (Carling et al., 2000a; Kleinhans et al., 2002; Venditti et al., 2019) and measurements do not indicate a clear evolution in time. Same difficulty arises when modelling the problem in the flume. The laboratory experiments of Tuijnder et al. (2009) show dune dimensions that progressively decrease as the volume of the finer mobile sediment decreases and the immobile coarser underlayer is exposed. In contrast, the experimental data of Porcile et al. (2020) describe starved dunes attaining longer wavelengths than their alluvial counterparts for the same values of the hydrodynamic and morphodynamic parameters.

A first theoretical, process-based approach to the study of sand dune formation was proposed by Kennedy (1969), who introduced the idea that fluvial dunes can be the result of a free instability of a uniform steady flow over an alluvial bed. In the following decades, several researchers investigated the formation of dunes and ripples by means of a linear stability analysis (Engelund, 1970; Reynolds, 1976; Richards, 1980; Colombini, 2004; Colombini and Stocchino, 2011). An extensive review of the linear stability analyses of alluvial bed forms can be found in Colombini and Stocchino (2012).

All these theoretical investigations consider an infinite availability of mobile sediment and thus they are invalid in the case of sediment starvation. Blondeaux et al. (2016) and Porcile et al. (2017) investigated the effects of sediment starvation on the formation of sea-wave ripples and tidal dunes, respectively. They simulated the formation of small-amplitude starved bedforms in oscillatory currents by means of an idealised model based on a stability analysis. Here a similar theory is developed for steady currents, which can be considered as an extension of the linear stability analysis of Colombini (2004) including the effect of sediment starvation. Our main hypothesis is that when a motionless substratum is exposed by the formation of dunes, the lack of sand affects the sediment transport, and, in turn, the dune morphology. By following the modelling procedure outlined in Blondeaux et al. (2016), this hypothesis is formulated through numerical means.

We apply this model to the formation of laboratory-scale sand dunes by assuming hydrodynamic and sediment transport parameters in line with flume experiments previously performed at the University of Genoa (Porcile et al., 2020). Model results describe the lengthening of starved dunes with an increasing irregularity in their spacing as their growth progressively exposes the unerodible substratum.

Secondly, we dropped the limiting assumption of small dune amplitudes with respect to the local water depth, which is implicit in the linearization process, by performing a fully numerical modelling of finite-amplitude starved dunes. We developed an application of the commercial model Delft3D capable of describing the formation of sand dunes in steady currents while accounting for sediment starvation. Analogously to the small-amplitude dune model, the presence of a motionless substratum is included that can lead to sediment starvation depending on initial sediment availability and forcing conditions. Numerical results confirm the findings of the linearized solution, thus suggesting that the lack of sediment available for transport dictates the

dimensions of fluvial dunes, potentially affecting the frictional force they exert on the overlying flow.

This paper is organised as follows. Section 2 is devoted to a brief description of the experimental measurements of Porcile et al. (2020) that we used to provide controlled empirical fundations for the development of process-based idealised models of the genesis of sand-starved dunes in steady currents. In section 3.1 we formulate a stability analysis of sandy beds forced by steady currents considering a limited availability of mobile sediment. In section 3.2 we introduce a fully numerical model of the formation of finite-amplitude starved dunes. Section 4 present the results of our modelling exercises. Then, these results are thoroughly compared with previous laboratory measurements and field observations in section 5. Conclusions are drawn in section 6.

2 Background: Flume experiments by Porcile et al. (2020)

Porcile et al. (2020) described experimental measurements of the formation of starved dunes carried out in a laboratory flume at the University of Genoa. These flume experiments were designed to provide further data on the effects of sediment starvation on the formation of fluvial dunes and to compare results of the present numerical investigation with laboratory measurements. Three sets of experiments were performed by fixing all the hydrodynamic and morphodynamic parameters, except the thickness of the layer of sediment initially available for transport. The duration of the experiments was also kept constant. Well-sorted sand characterised by a mean grain size $d_s^* = 1.12\ mm$ was glued on the bottom of the flume, thus creating a rough bed. Before water was pumped through the flume, the same sand was spread on the rough fixed bottom, generating a sand layer with an initial uniform thickness Δ^*, that can be varied per experiment. This setup allowed us to investigate the effects of sediment starvation alone by progressively decreasing the thickness of the initial sand layer (see Porcile et al. (2020) for additional details on the apparatus and experimental procedure).

The bed elevation recorded at the end of the experiments along the centerline of the flume shows that well-defined sand dunes emerged from a uniform sand layer independently on the initial sediment availability (Figure 1). When the emerging bedforms were not high enough to expose the unerodable bottom of the flume, bed profiles of alluvial dunes were observed (Figure 1-top). Average wavelengths of these alluvial dunes were approximately the same during all the experiments, showing triangular shapes with gentle stoss sides and steep lee sides. As soon as the growth of the dunes led to the exposure of the flume bottom, regularly spaced transverse dunes were replaced by bump-shaped starved bedforms with steep stoss and lee sides separated by flat troughs (Figure 1-middle and 1-bottom).

Crest-to-crest distances of starved dunes markedly increased when starting off with a thinner initial sand layer. An increasing irregularity associated to a decreasing thickness of the initial sand layer was also observed. In some cases, the strongest sediment starvation resulted in the

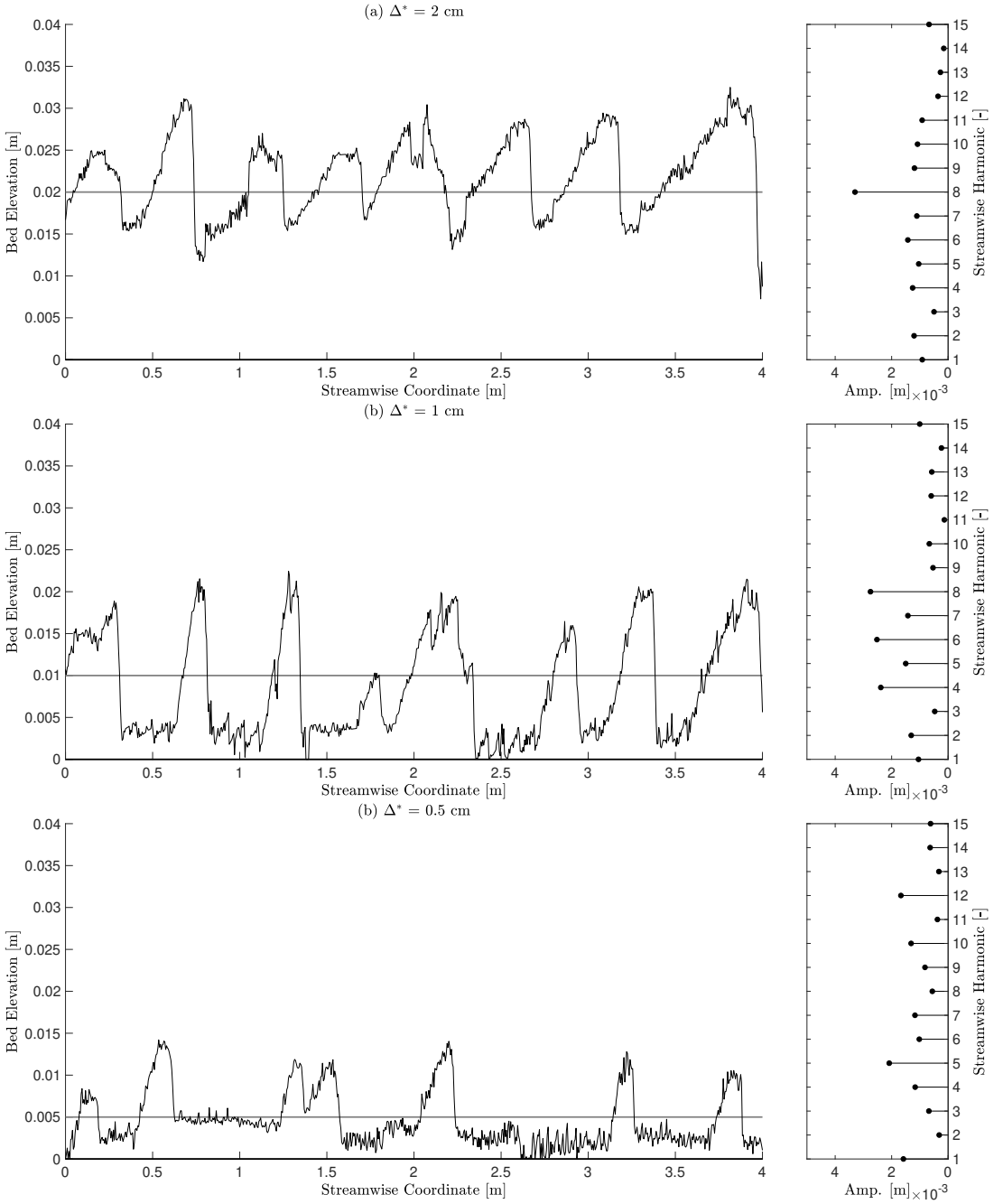

Figure 1: Laboratory measurements of Porcile et al. (2020). Left panels: final bottom configurations measured along the centerline of the flume for decreasing values of the initial uniform thicknesses of the sand layer $\Delta^* = 2$ cm (top), $\Delta^* = 1$ cm (middle) and $\Delta^* = 0.5$ cm (bottom). Forcing flow direction is from left to right. Thin black lines represent the bed elevations, thick black lines show the rigid bottom of the flume while thick grey lines show the initial level of the sand layer. Right panels: Spectra of the final bottom configurations. The amplitude of the Fourier components is plotted versus the streamwise harmonic.

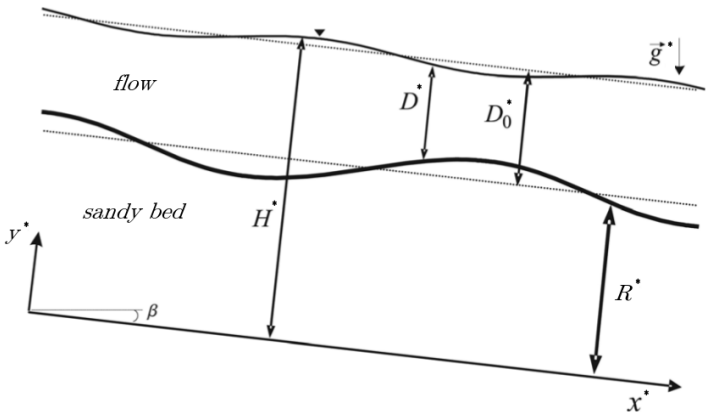

Figure 2: Sketch of the hydrodynamic modelling showing the sloping streamwise x^*-axis, the almost vertical y^*-axis pointing upwards, the local water depth D^* and the reference level R^*.

appearance of three-dimensional barchan dunes. The lengthening of starved bedforms is also shown by the Fourier spectra of the bottom profiles (Figure 1 right panels), which provide a measure of the increasing spacing of starved dunes and allow for a rough estimation of their average wavelength. Streamwise profiles of alluvial dunes were characterised by peak harmonic components corresponding to approximately 0.5 m average wavelength. The spectra of starved dunes show that the peak harmonic component shifts towards lower frequencies as the initial availability of sediment decreases, confirming their marked lengthening.

3 Methods

Here we describe both the quasi-linear model (subsection 3.1), whereby a linear flow model provides the stress field, a predictor relationship computes the associated sediment transport and the Exner equation is integrated numerically including the effect due to sediment starvation, and the fully nonlinear Delft3D model (subsection 3.2).

For both models, the flow of an incompressible fluid in a wide straight channel is considered and the Reynolds averaged Navier Stokes (RANS) equations on a vertical plane (2DV) together with the 1D form of the Exner equation are used to describe the hydrodynamics and the bed evolution, respectively.

3.1 Quasi-linear model

By adopting the so-called quasi-steady approximation, whereby the flow is assumed to adapt instantaneously to variations of the bed elevation, the solution of the morphodynamic problem can be split in two parts: i) the solution of the steady flow equations above a fixed periodic bed, which provides the flow response to a given bed perturbation in terms of the stress acting on the bed; ii) the solution of the Exner equation, which provides the evolution of the bed perturbation

in terms of propagation and amplification. An algebraic empirical relationship provides the link between these two steps, relating the local value of the net sediment transport to the local value of the stress acting on the bed.

In the quasi-linear model, at any given time, the spatially periodic bed topography is decomposed in a finite number of harmonics. Moreover, the amplitudes of the bed harmonics are assumed to remain small enough for the linear approximation to hold, so that the flow field is expressed as the superposition of the (linear) flow response to each of the bed harmonics. The bed stress distribution provided by the hydrodynamic module is then fed to the morphodynamic module, where the stress field is converted in a sediment discharge distribution. If part of the motionless substratum is exposed, a suitable numerical procedure is then employed, which corrects the sediment transport rate to account for the local unavailability of erodible sediment. Finally, the new bed topography is evaluated by means of a numerical integration of the Exner equation.

3.1.1 Hydrodynamic module

The formulation of the hydrodynamic module follows closely the one adopted by Colombini (2004) and by Colombini & Stocchino (2005, 2008), which is briefly summarized in the following. The interested reader is referred to the above works for the details of the flow model.

A steady, turbulent free-surface flow is considered in the domain sketched in Figure 2, whereby the streamwise x^*-axis is sloping with slope $S \equiv \tan(\beta)$ and the almost vertical y^*-axis points upwards (hereinafter an asterisk denotes dimensional quantities). The free-surface is represented by the curve $y^* = R^* + D^*$, where D^* is the local water depth and R^* indicates the reference level, i.e., the average level at which conventionally the mean logarithmic velocity profile vanishes. This level represents the interface between the fluid flow and the river bed and depends primarily on the bottom roughness.

The triplet composed by the (constant) fluid density ρ^* and by the uniform flow depth D_0^* and shear velocity $u_{\tau 0}^*$ is used for nondimensionalization.

Neglecting the viscous stresses, the steady, dimensionless 2DV RANS and continuity equations read

$$U\frac{\partial U}{\partial x} + V\frac{\partial U}{\partial y} = -\frac{\partial P}{\partial x} + \frac{SC^2}{\mathrm{Fr}^2} + \frac{\partial T_{xx}}{\partial x} + \frac{\partial T_{xy}}{\partial y} \ , \tag{1}$$

$$U\frac{\partial V}{\partial x} + V\frac{\partial V}{\partial y} = -\frac{\partial P}{\partial y} - \frac{C^2}{\mathrm{Fr}^2} + \frac{\partial T_{xy}}{\partial x} + \frac{\partial T_{yy}}{\partial y} \ , \tag{2}$$

$$\frac{\partial U}{\partial x} + \frac{\partial V}{\partial y} = 0 \ , \tag{3}$$

where P is the ensemble-averaged pressure and (U, V) are the ensemble-averaged velocity components in the x and y directions, respectively. Moreover, T_{ij} are the dimensionless Reynolds

stresses

$$\mathbf{T} = \begin{bmatrix} T_{xx} & T_{xy} \\ T_{yx} & T_{yy} \end{bmatrix} = \begin{bmatrix} 2\nu_T \frac{\partial U}{\partial x} & \nu_T \left(\frac{\partial U}{\partial y} + \frac{\partial V}{\partial x} \right) \\ \nu_T \left(\frac{\partial U}{\partial y} + \frac{\partial V}{\partial x} \right) & 2\nu_T \frac{\partial V}{\partial y} \end{bmatrix} , \tag{4}$$

and ν_T is the dimensionless turbulent eddy viscosity.

Two parameters are generated by the nondimensionalization procedure, namely the Froude number $\mathrm{Fr} = U_0^*/\sqrt{g^* D_0^*}$ and the conductance coefficient $C = U_0^*/u_{\tau 0}$, where U_0^* is the area velocity of the base uniform flow and g^* is the gravitational acceleration. These two parameters are related to one another by the uniform-flow law, yielding:

$$u_{\tau 0}^* = \frac{U_0^*}{\mathcal{C}} = \sqrt{g^* D_0^* S} \qquad \Rightarrow \qquad \mathcal{C} = \frac{U_0^*}{u_{\tau 0}^*} \simeq \frac{\mathrm{Fr}}{\sqrt{S}} . \tag{5}$$

Furthermore, the coordinate transformation

$$\xi = x , \qquad \eta = \frac{y - R(x)}{D(x)} , \tag{6}$$

is introduced, which maps the flow domain of Figure 2 into a rectangular domain.

The turbulent eddy viscosity ν_T is expressed in terms of an algebraic mixing length L as

$$\nu_T = \frac{1}{D} \frac{\partial U}{\partial \eta} L(\eta)^2 \quad , \qquad L(\eta) = \kappa D(\eta + \eta_R)(1 - \eta)^{1/2} \quad , \qquad \eta_R = \frac{2.5 d_s}{30}, \tag{7}$$

where η_R is the roughness height, which is assumed to be proportional to the non dimensional roughness and, ultimately, to the dimensionless sediment diameter d_s.

The problem is then closed by an appropriate set of boundary conditions. In particular, at the reference level the velocity components vanish according to the no-slip condition

$$U = 0 \quad , \quad V = 0 \quad \text{at} \quad \eta = 0 , \tag{8}$$

whereas at the free surface, the kinematic boundary condition reads

$$-U \left(\frac{\partial R}{\partial x} + \frac{\partial D}{\partial x} \right) + V = 0 \quad \text{at} \quad \eta = 1 . \tag{9}$$

and the dynamic boundary condition yields

$$T_N = 0 \quad , \quad T_T = 0 \quad \text{at} \quad \eta = 1 , \tag{10}$$

where T_N and T_T represent the normal and tangential components of the stress acting on a surface at constant η, respectively. Finally, periodic boundary conditions are enforced at the upstream and downstream sides of the domain.

3.1.2 Perturbation method

Assuming that the height of the dunes is much smaller than the local water depth, the flow field can be evaluated by means of a perturbation approach. As far as the formation of regularly spaced dunes is concerned, it is also possible to assume the periodicity of the bottom geometry. The sandy bed can then be expressed as superposition of different spatial components. Of note, with the goal of extending the analysis to starved dunes, the number of spatial components should be large enough to properly describe those transition regions where the exposition of the unerodible substratum occurs. Presently, the following normal-mode representation for the perturbed variables is adopted

$$F(\xi,\eta) = F_0(\eta) + \epsilon F_1(\xi,\eta) = F_0(\eta) + \epsilon f(\eta) e^{i\alpha\xi} + c.c., \tag{11}$$

where ϵ is a small parameter and α denotes the longitudinal dimensionless wavenumber of the perturbation.

Substituting the above splitting into the system of equations (1)-(3) and boundary conditions (8)-(10) and collecting terms at the same order of magnitude in ϵ, a set of ordinary differential equations is derived at $\mathcal{O}(\epsilon)$. The resulting two-points boundary value problem is eventually solved by means of a shooting method. In particular, the flow response to a perturbation of the bed of amplitude r can be determined in terms of the shear stress t_{tb} evaluated at the saltation level η_B, which represents the interface between the flowing fluid and the saltation layer, i.e., the thin bottom layer were bedload transport takes place (Colombini, 2004). Moreover, the saltation level is assumed parallel to the reference level at a distance equal to the bedload layer thickness

$$\eta_B - \eta_R = l_B d_s = \left\{ 1 + a_B \left(\frac{T_{TR} - T_{TC}}{T_{TC}} \right)^{m_B} \right\} d_s. \tag{12}$$

where T_{TR} and T_{TC} are the shear stress evaluated at the reference level and its critical threshold for incipient motion. The empirical parameters a_B, m_B have been set equal to 1.42 and 0.64, respectively (Colombini and Stocchino, 2008).

As expected from a linear, normal-mode analysis, we eventually obtain:

$$t_{tb} = t_t(\eta_B) = r\ \widehat{t}_{tb} \tag{13}$$

where $\widehat{t}_{tb}$ only depends on the wavenumber α and on the flow parameters Fr and C (see Colombini (2004) for the details of the above procedure).

3.1.3 Morphodynamic module

In the present formulation, suspended sediment transport is neglected and only bed-load transport is considered, i.e., sliding, rolling and saltating grain particles. Such an assumption seems reasonable since sand dunes are more likely to appear in sub-critical flows (Fredsøe, 1974), the

bottom shear stress generated by which do not usually produce large suspension of sediment. A common and useful approach to the quantification of bedload transport is to empirically relate the volumetric sediment transport rate per unit width q_S^* with the difference between the bottom shear stress T_{TB}^* and the critical threshold value for incipient motion T_{TC}^*. A large number of empirical relations have been derived using flume data from many laboratory experiments, and these share the structure

$$\frac{q_S^*}{\sqrt{(s-1)g^* d_s^{*3}}} = \Phi(\Theta_B, \Theta_C) \ , \tag{14}$$

where $s = \rho_s^*/\rho^*$ is the relative density of the sediment, Φ is the dimensionless bed-load transport rate and Θ_B is the Shields parameter built upon the bed shear stress at level B. More precisely, we have:

$$\Theta_B = \frac{T_{TB}^*}{g^*\rho^*(s-1)d_s^*} = T_{TB}\Theta_{R0} \ , \qquad \Theta_{R0} = \frac{S}{(s-1)d_s} \ , \tag{15}$$

where Θ_{R0} is the Shields parameter evaluated at the reference level for the base uniform flow.

Among the commonly adopted bed-load transport predictors is the Fernandez Luque and Van Beek (1976) formula, which reads

$$\Phi = 5.7\,(\Theta_B - \Theta_C)^{3/2} \quad \text{if} \quad \Theta_B > \Theta_C \ , \Phi = 0 \quad \text{if} \quad \Theta_B \simeq \Theta_C \ . \tag{16}$$

This predictor relation is presently employed as it appears to contain the main physical ingredients controlling the process of sediment transport for values of the Shields parameter close to its threshold. Furthermore, the bed material tested in the experiments, on which the above relation is based, included different grain sizes ranging from sand to gravel.

Since the problem under consideration accounts for the presence of bottom perturbations, the bed is not flat and the stabilising effect of gravity, which opposes uphill motion and favours downhill motion, is considered by correcting the threshold Shields stress Θ_C (Fredsøe and Deigaard, 1992)

$$\Theta_C = \Theta_{CH}\left[1 - \left(S - \frac{\partial B}{\partial \xi}\right)\frac{1}{\mu_d}\right] \ , \quad \text{with} \quad \Theta_{CH} = 0.038 \ , \tag{17}$$

where Θ_{CH} is the value for vanishing slope and μ_d is a dynamic friction coefficient, which has been set equal to one half of the Coulomb coefficient μ_c following the recommendations by Fredsøe and Deigaard (1992). Moreover, $\mu_c = \tan(\Psi)$ and Ψ represents the angle of repose of the sediment. For natural sediments, the angle of repose Ψ ranges between 30° and 50° resulting in friction coefficient μ_c ranging between 0.58 and 1.2. In this study we have employed $\mu_c = 1.0$.

Finally, the development of small-amplitude bottom perturbations can be estimated by the sediment continuity equation, which states that the positive (negative) divergence of the sediment transport rate is locally balanced by the decrease (increase) of the bottom elevation

$$\frac{\partial R}{\partial T} = -\frac{\partial \Phi}{\partial \xi} \ , \qquad T = \frac{t^*\sqrt{(s-1)g^* d_s^{*3}}}{D_0^{*2}(1-p)} \ , \tag{18}$$

where T is a slow morphodynamic time coordinate.

3.1.4 Linearization

Under the hypothesis of small amplitude bed perturbations, the algebraic relationships (15-17) can be linearized, providing the linear response of the flow to a given bed perturbation in terms of the equilibrium (at capacity) sediment discharge.

In particular, we expand the bedload discharge Φ, the Shields parameter Θ_B and its critical value Θ_C as in (11)

$$\Phi(\xi) = \Phi_0 + \epsilon\phi e^{i\alpha\xi} + c.c. \ , \tag{19}$$

$$\Theta_B(\xi) = \Theta_{B0} + \epsilon\theta_b e^{i\alpha\xi} + c.c. = \Theta_{R0}\left[1 - \eta_B + \epsilon t_{tb} e^{i\alpha\xi} + c.c.\right] \ , \tag{20}$$

$$\Theta_C(\xi) = \Theta_{C0} + \epsilon\theta_c e^{i\alpha\xi} + c.c. = \Theta_{CH}\left[1 - \frac{S}{\mu_d} + \epsilon i\alpha\frac{1}{\mu_d} r e^{i\alpha\xi} + c.c.\right] \ . \tag{21}$$

At the leading order in ϵ, we eventually obtain

$$\phi = \left(\frac{\partial\Phi}{\partial\Theta_B}\right)_0 (\theta_b - \theta_c) = \left(\frac{\partial\Phi}{\partial\Theta_B}\right)_0 \left(\Theta_{R0}\widehat{t}_{tb} - \Theta_{CH}\frac{i\alpha}{\mu_d}\right) r = \widehat{\phi} r \tag{22}$$

where, as for (13), the complex quantity $\widehat{\phi}$ only depends on the wavenumber α and on the flow and the sediment parameters for the base state.

Let us now consider the case of infinite availability of sediment, which corresponds to a motionless unerodible substratum low enough for not being exposed by the erosive action of the flow. In this case, with the additional hypothesis of small amplitude of the bed perturbation, the Exner continuity equation (18) can be linearized and the classic normal mode stability analysis is recovered. To this end, the reference level R is expanded as

$$R(\xi, T) = R_0 + \epsilon R_1(\xi, T) = R_0 + \epsilon r(T) e^{i\alpha\xi} + c.c. \tag{23}$$

and substituted in (18) to obtain the dispersion relationship

$$\frac{1}{r}\frac{dr}{dT} = -i\alpha\frac{\phi}{r} = -i\alpha\widehat{\phi} \quad \Rightarrow \quad r(T) = e^{-i\alpha\widehat{\phi}T} = e^{\Omega T} e^{-i\alpha\omega T} \ , \tag{24}$$

where $\widehat{\phi}$ represents the complex wavespeed of the perturbation and

$$\omega = \mathrm{Re}\left(\widehat{\phi}\right) \ , \qquad \Omega = \alpha \mathrm{Im}\left(\widehat{\phi}\right) \ , \tag{25}$$

are the celerity and growth rate of the bed perturbation, respectively.

An exponential dependence of the solution on time emerges, as expected in a linear stability

analysis. The growth rate is found to be

$$\Omega = \alpha^2 \Theta_{R0} \left(\frac{\partial \Phi}{\partial \Theta_B} \right)_0 \left(\frac{\mathrm{Im}\left(\widehat{t}_{tb}\right)}{\alpha} - \frac{\Theta_{CH}}{\Theta_{R0}\mu_d} \right) , \tag{26}$$

which clearly shows how the emergence of small-amplitude dunes is related to a balance between the destabilising effect due to the steady current, represented by the shear stress at the bed-load level, and the stabilising effect due to the gravity, represented by the dynamic friction coefficient. Thus the study of the dispersion relationship allows growing modes with positive growth rate to be identified in the parameter space and, among those, the fastest growing one. Finally, an estimate of the wavelength of the emerging dunes can be predicted by assuming that this most unstable mode prevails on the others during the short-term morphodynamic evolution of the sandy bed.

3.1.5 Modification to account for sediment starvation

When a motionless substratum is exposed by the formation of sand dunes, the lack of sediment affects its transport, and, in turn, the pattern morphology. The exposure of the motionless substratum locally prevents the entrainment of sediment, leading to sediment starvation. The sediment transport formula (16) quantifying the bed-load sediment transport cannot be applied in the case of sediment starvation unless a suitable numerical procedure is introduced capable of account for the local lack of mobile sediment.

Where sand is available, the sediment transport depends only on the bed shear stress. If the shear decreases (increases) in the flow direction, the sediment transport rate can be predicted by the predictor formula and some deposition (erosion) occurs according to the continuity of the sediment phase. Differently, where a motionless substratum is locally exposed, the amount of sediment in motion might be smaller than the local transport capacity. In particular, the value of the sediment transport rate $\Phi(x^*)$ depends not only on the value of the shear stress $\Theta_B(x^*)$ but also on its spatial derivative. On the one hand, if the shear stress increases in the direction of the flow, the sediment transport rate remains constant since the flow cannot entrain additional mobile sediment since it is not available. On the other hand, if the shear stress decreases in the direction of the flow, two different scenarios are possible depending on the upstream value of the sediment transport rate. If the upstream value of the sediment transport rate is smaller than the local value predicted by the predictor formula $\Phi_P(x^*)$ the local sediment transport rate should be assumed equal to its upstream value. This can occur due to the upstream exposure of the motionless substratum. Otherwise, the sediment transport rate can be predicted by the predictor formula and some deposition of sediment over the exposed substratum should occur.

$$\left.\frac{d\Phi}{dx^*}\right|_+ = 0 \quad \text{if} \quad \left.\frac{d\Theta_B}{dx^*}\right|_{x^*} > 0 , \tag{27}$$

$$\left.\frac{d\Phi}{dx^*}\right|_{+} = 0 \quad \text{if} \quad \left.\frac{\Theta_B}{dx^*}\right|_{x^*} < 0 \quad \text{and} \quad \Phi(x^*) < \Phi_P(x^*) \ , \tag{28}$$

$$\Phi(x^*) = \Phi_P(x^*) \quad \text{if} \quad \left.\frac{\Theta_B}{dx^*}\right|_{x^*} < 0 \quad \text{and} \quad \Phi(x^*) > \Phi_P(x^*) \ . \tag{29}$$

These simple rules (27)-(29) introduce strong nonlinearities and the time development of the bottom configuration can be obtained only by numerical means. The present model integrates in time and space the dimensionless sediment continuity equation. The time advancement of (18) is solved by means of a Runge-Kutta second order approach, while the spatial derivatives are replaced by their second order finite difference approximations. A computational domain of length L_d^* along the horizontal axis x^* is considered and periodic boundary conditions are applied at its ends. The dimensionless length of the computational domain $L_d = L_d^*/D_0^*$ and the thickness of the initial sand layer $\Delta = \Delta^*/D_0^*$ are free geometrical parameters. The value of L_d should be large enough to assume its influence on the time development of the bottom configuration to be negligible and to properly represent the formation of the fastest growing mode predicted by the linear stability analysis. Since the time development of the entire range of unstable modes has to be described with sufficient accuracy, the spatial discretization should be accurate enough to represent the smaller wavelength of the unstable modes predicted by the linear stability analysis with a suitable number of computational points.

In those transition regions between the motionless substratum and the erodible bed, small-scale spurious oscillations arise as a result of the Gibbs' effect associated with the discontinuity in the bed slope. In its numerical time-stepping, the model forces the bed elevation to never drop below the substratum's level by applying a filtering procedure removing the small-scale spurious oscillations. The results of preliminary simulations repeated halving grid size, time step and domain length indicate that the chosen couple of values does not affect the time development of the bottom configuration.

3.2 Fully nonlinear model

3.2.1 General model description

The finite-amplitude evolution of fluvial dunes in sediment scarce environments is modelled in the numerical shallow water model Delft3D (Lesser et al., 2004). Analogous to the small-amplitude model, the hydrodynamic equations (here in terms of vertical σ-coordinates) consist of the 2DV Navier Stokes equations, a continuity equation and a turbulence closure model, supplemented by appropriate boundary conditions. In contrast to the small-amplitude model, turbulence is modelled by means of the $k_T - \epsilon_T$ turbulence model, in which both the turbulent kinetic energy per unit volume k_T and the dissipation rate per unit volume ϵ_T are computed. Both the bed load and the suspended load are included in the model, and bed evolution is computed by the Exner equation. For an overview of the relevant 2DV model equations, see e.g. Damveld et al.

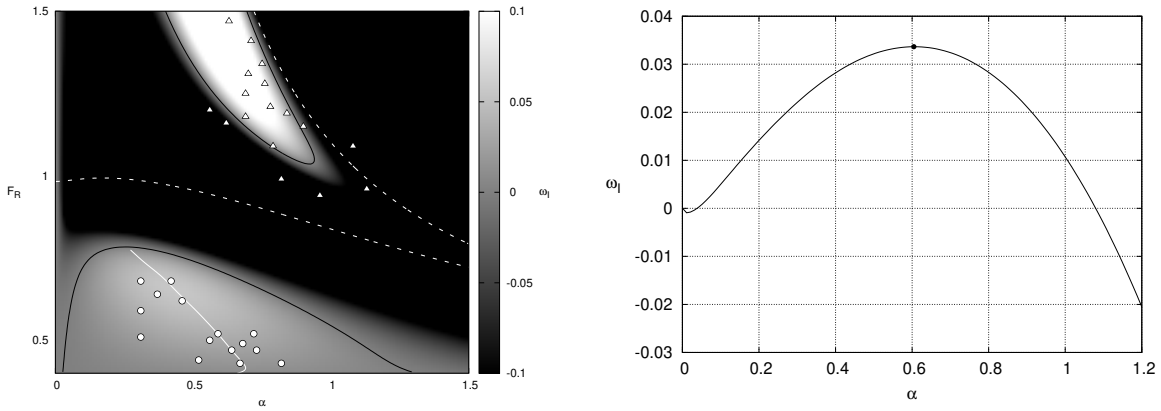

Figure 3: Results of the quasi-linear model in the case of an unlimited sediment supply. Left panel: growth rate plotted in shades of grey for a value of the conductance coefficient $\mathcal{C} = 15$. Thick black lines represent the curves of vanishing growth rate, dashed white lines represent the curves of vanishing celerity, white line represent fastest growing modes. The marks indicate the experimental measurements of Guy et al. (1966): circles, dunes; triangles , antidunes. Right panel: growth curve for a value of the Froude number Fr = 0.5 whose maximum identifies the fastest growing mode.

(2020).

3.2.2 Model domain, boundary conditions and parameter choices

The horizontal length of the domain is 60 m long and has a uniform grid spacing of 2.5 cm. In the vertical direction the grid consists of 30 σ-layers, with a small thickness (0.25% of the local water depth D^*) near the bed, gradually increasing in the upward direction. At the upstream lateral boundary a logarithmic velocity profile with a constant discharge of 0.03 m^3/s is specified, whereas at the downstream lateral boundary the water level is kept constant throughout the simulations at a level of 12 cm. These values lead to a Froude number Fr = 0.51, similar to those characterising the flume experiments. The vanishing of the stress tensor was imposed at the free surface. The area of interest is situated in the second half of the domain to ensure that possible upstream boundary disturbances do not migrate into the domain and influence the results. The hydrodynamic time step is set equal to 0.15 seconds and a spin-up time of 10 minutes is made during which no bed level changes are allowed. Finally, the roughness of the bed is specified through a roughness length z_0 of 1 mm, which is equal to the sediment diameter. Note that the bed roughness does not change when the bare substrate is exposed, which is in fact in line with the experimental setup, where sediment was glued to the bottom of the flume (Porcile et al., 2020).

4 Results

Generally, comparing theoretical results of stability analyses with laboratory measurements is difficult. Since the flume width is usually of the same order of the flow depth, the side walls affect the bottom shear stress. If the bottom is rougher than the side walls, as in the experiments by Porcile et al. (2020), the distribution of the shear along the wetted perimeter of the channel is nonuniform. As such, experimental outcome cannot be expected to correspond to theoretical findings based on the assumption of a wide open-channel flow, unless a correction for the shear stress at the side walls is made. An equivalent, uniform open-channel flow characterising the flume experiments can be evaluated by the side-wall correction (Vanoni and Brooks, 1957). Partitioning the flume cross-section into a hydraulically rough and a smooth sub-regions corresponding to the bottom and the side walls, respectively, and solving iteratively a system of implicit equations including the water continuity, the Keulegan equations for smooth and rough flow regimes and the Rouse equation, the side-wall correction determines a uniform, wide open-channel flow, which is related to the uniform flow realised in the narrow flume. Then, it is possible to evaluate its principal unknowns of interest. Particularly useful for a comparison with the linear stability analysis is the equivalent Froude number and the representative conductance coefficient. It is worth nothing that the Froude numbers characterising the equivalent open-channel flows related to the individual experiments turn out to be larger than their measured values. This experimental post-process is crucial to generalise the results of lab-scale flows by defining global dimensionless quantities of interest which are independent of the flume width. As such, the side-wall correction allows for comparing the experimental results with the modelling of small-amplitude dunes.

4.1 Quasi-linear model results

The investigation of the dispersion relationship (23) allows possible instability regions to be isolated in the parameter space. Among the free parameters of the stability-based model, there are the unperturbed flow depth D_0^* and the uniform mean grain size of the sediment d_s^*, which determine the conductance coefficient characterising the unperturbed steady stream. In order to compare the laboratory observations with the average wavelength of small-amplitude alluvial dunes predicted by the stability analysis, the value of the mean grain size was set equal to that of the well-sorted sediment used in the experiments. The unperturbed mean water depth was set equal to the uniform depth of the wide open channel flow evaluated by the side-wall correction. Then, the values of the conductance coefficient and the Froude number can be easily evaluated ($\mathcal{C} = 15, \mathrm{Fr} = 0.5$) for the unperturbed flow.

Varying the Froude number, it is possible to compute the growth rate ω_I as well as the value of ω_R which determines the perturbation celerity as function of the dimensionless wavenumber α (see Figure 3). Positive values of the growth rate represent the growth of small-amplitude perturbations, thus indicating instability. On the other hand, the value of ω_R determines the perturbations' celerity, positive (negative) values indicating downstream (upstream) migration.

In left panel of Figure 3 the broken white lines represent vanishing values of the migration rate. Below the lower broken line the celerity of the growing modes is positive (i.e. downstream migration, alluvial dunes). The growing modes lying above this line has negative celerity (i.e. upstream migration, alluvial antidunes). The good agreement between the identified regions of instability and the experimental dataset of Guy et al. (1966) later śide-wall corrected' by Colombini (2004) prove the reliability of the stability analysis. Our experimental data fall within the appropriate region of instability corresponding to some of the smaller (wavelengths) dunes observed by Guy et al. (1966).

From the previous plot in the left panel of Figure 3, it is possible to extrapolate the growth curve shown in the right panel of Figure 3 by considering the value of the Froude number of the experiments. Hence, the fastest growing mode can be selected among the range of the predicted perturbations. Assuming that this mode prevails over the short-term morphodynamic evolution of the sandy bed, the wavelength of the small-amplitude dunes can be predicted. For the chosen set of parameters the stability analysis predicts the appearance of bottom perturbations characterised by a wavenumber $\alpha = 0.6$, which corresponds to a value of the dimensional wavelength slightly smaller than $\lambda^* = 1\ m$. This value is of the same order of the wavelengths of the alluvial dunes observed during the experiments, though an overestimation is present.

To test whether the model can provide a reliable description of the genesis of small-amplitude starved dunes as observed during the flume experiments, a series of simulations is performed computing the time development of an initial random bottom waviness forced by a uniform steady current by fixing the hydrodynamic and morphodynamic parameters and varying only the supply of sediment. Analogously to the experimental investigation, the sediment supply is decreased by decreasing the thickness Δ of the initial sand layer through which dunes can develop. Figure 4 shows the bottom configurations at the beginning (grey lines) and at the end (black lines) of each numerical simulation. The values of the Froude number and the conductance coefficient are kept constant during all the numerical simulations and equal to those of the experiments evaluated by means of the side-wall correction. The dimensionless length L_d of the computational domain is equal to 100 and the dimensionless thickness of the initial sand layer is progressively decreased starting from $\Delta = 0.2$ down to $\Delta = 0.05$. Since the experiments are characterized by a dimensional mean water depth $D_0^* = 0.1$ m, the value of Δ^* ranges from 2 cm to 0.5 cm and the dimensional length of the computational domain is about 10 metres. Each numerical simulation is made considering a dimensionless simulation time that is of the same order of magnitude as that of the experiment duration. At the beginning of the first simulation (Figure 4, panel A) the bottom is characterised by a random perturbation of small amplitude. Then, the computed bottom profile shows a rapid decay of the perturbation components of very small wavelengths and only the unstable modes predicted by the stability analysis survive. Then, for long time, the growth of the fastest growing mode gives rise to periodic bedforms (dunes). The growth of dunes is exponential and for $\Delta = 0.2$, the appearance of the bottom forms does not bare the motionless substratum. At the end of the simulation, ten clearly defined dunes can

be easily identified through the computational domain with an average dimensional wavelength equal to ten. Different results are obtained in the second and third simulations (see panels B and C of 4). These results correspond to a dimensionless initial sand layer thickness equal to 0.1 and 0.05, respectively. Progressively decreasing the amount of the sediment available for transport, the motionless substratum is exposed by the growth of the dunes, leading to sediment starvation. Starved dunes show increasing crest-to-crest distances as the degree of sediment starvation increases. Their general lengthening and the increasing irregularity of their profile is evident.

The panels on the right-hand side of Figure 4 show one-dimensional spectra of the final bottom profiles computed by the stability-based model. The modulus of the complex amplitude of each harmonic component of the Fourier transform of the bottom elevation is presented. These spectra reveal whether a dominant wavelength can be identified or whether the bottom configuration is the result of a superposition of many different components. By comparing the harmonic content of each computed bed profile, it is seen that the peak harmonic component shifts towards lower frequencies as the thickness of the initial sand layer decreases.

4.2 Fully nonlinear model results

Next, we repeat our numerical experiments with the finite-amplitude model. Again, the only parameter which is varied is the initial sediment thickness. Figure 5 (left-hand panels) show the initial and final bottom configurations of the simulations. For the sediment abundant case (panel a), asymmetrically-shaped dunes develop, with an average crest-to-crest distance slightly larger than $\lambda^* = 1m$. Similar to the small-amplitude result, this value is of the same order as that observed during the experiments. Panels (c) and (e) of Figure 5 show a decreasing number of dunes as a result of the decreasing sediment availability. In contrast to the small-amplitude result, the wave height and spacing of the patterns become more regular over time, especially in the sediment scarce case. This is a good indication that the bottom configuration is close to their equilibrium state. Another effect which can be observed towards the end of the simulations is the decrease of asymmetry of the (isolated) bedforms, which are characterized by a shorter stoss side.

Similar to the results of the small-amplitude simulations, the right-hand panels of Figure 5 show the moduli of the Fourier components. Also in this case, it can be observed that the peak shifts towards the lower wavenumbers as the sediment thickness decreases. However, this observation is less apparent than in the former case. Due to asymmetrical shape of the patterns, the harmonic signal is composed of a much broader spectrum, such that no particular peak stands out.

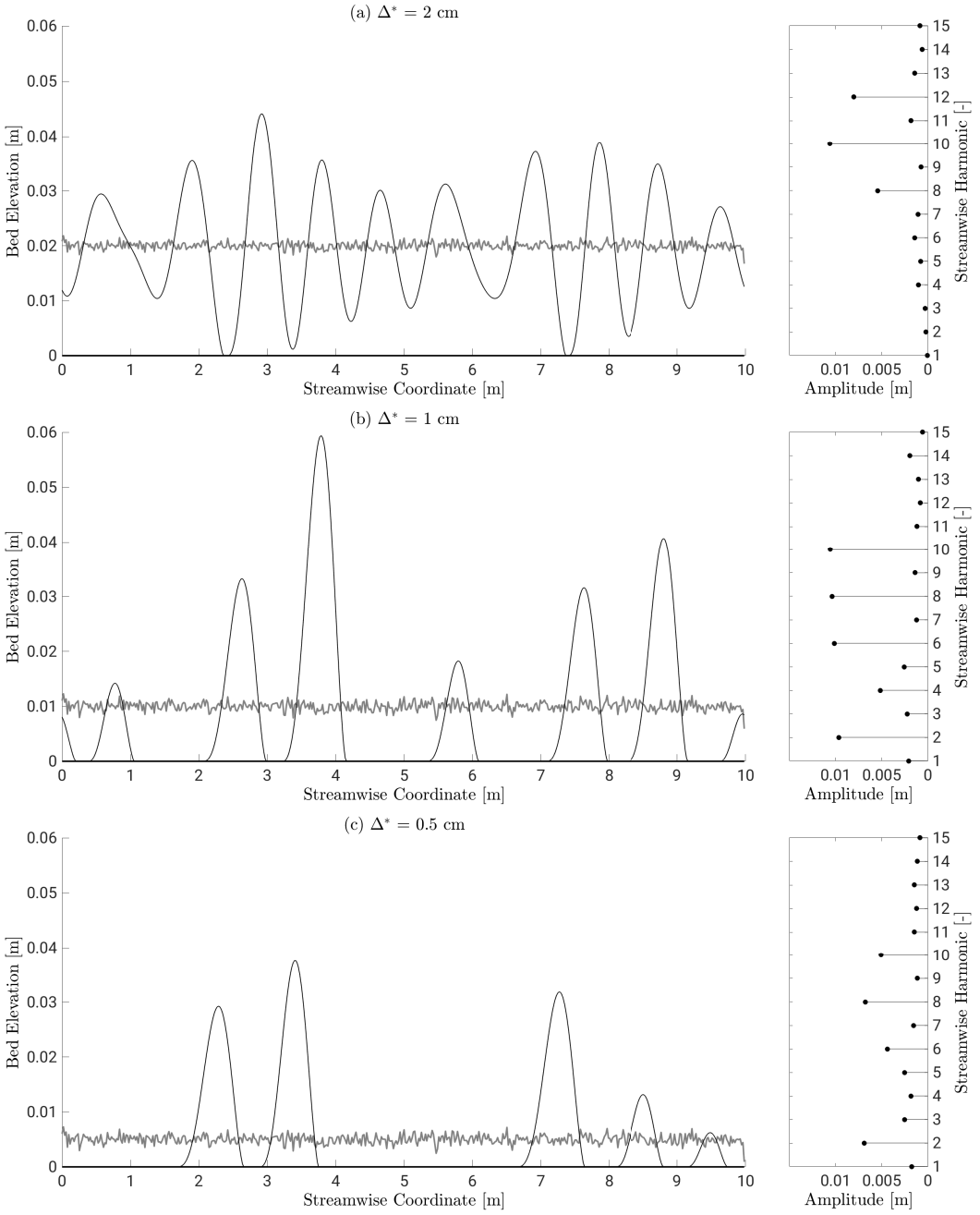

Figure 4: Results of the quasi-linear model in the case of a limited sediment supply. Left panels: Time development of an initial random bottom waviness for the values of dimensionless parameters $\mathcal{C} = 15$ and $\mathrm{Fr} = 0.5$ and decreasing values of initial uniform thicknesses of the sand layer. Thin black lines represent the final bottom configurations computed by the model, thick black lines show the motionless bottom while thin grey lines show the initial random waviness. Right panels: Spectra of the final bottom configurations. The amplitude of the Fourier components is plotted versus the streamwise harmonic.

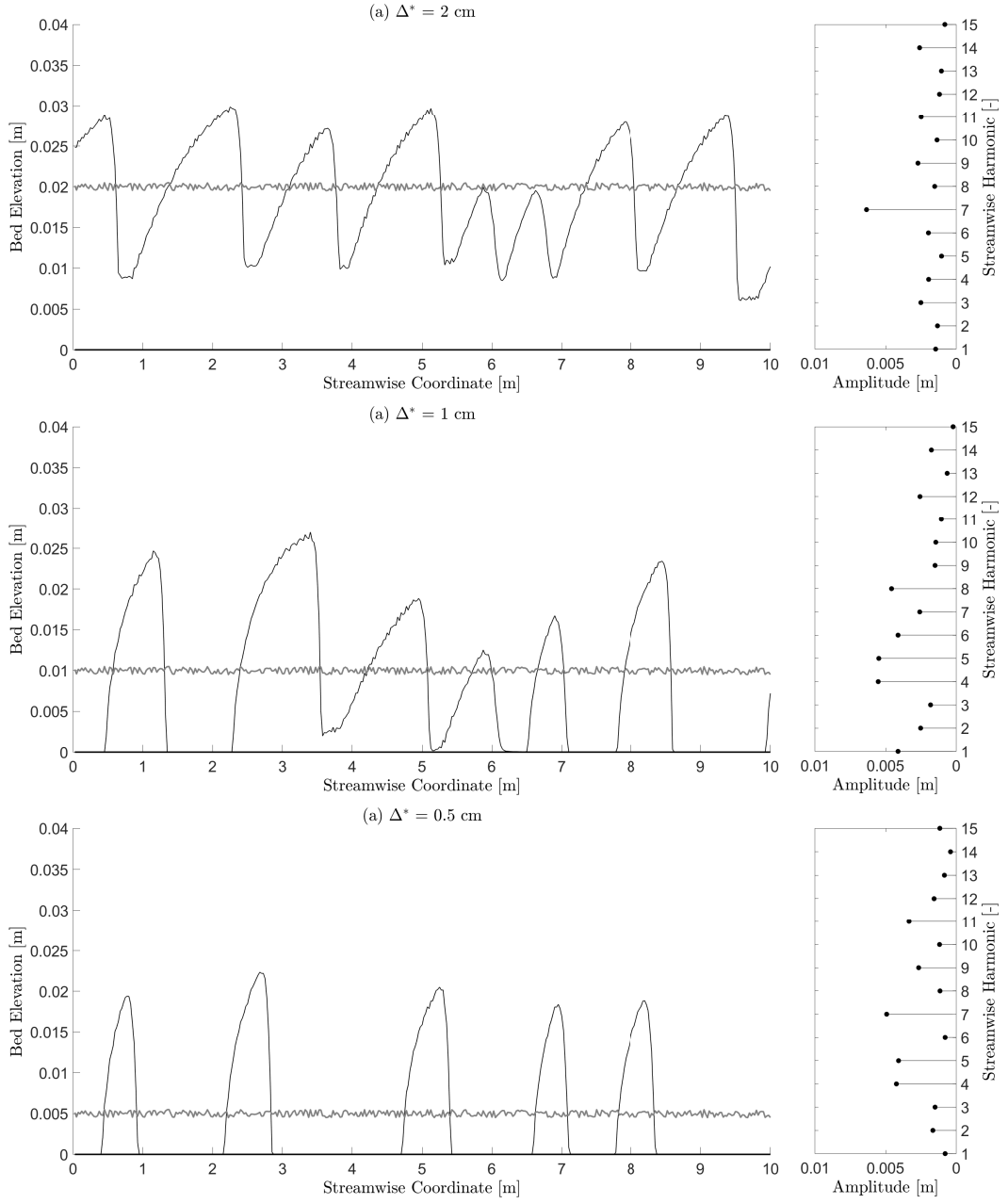

Figure 5: Results of the fully nonlinear Delft3d model in the case of a limited sediment supply. Left panels: Time development of an initial random bottom waviness decreasing values of initial uniform thicknesses of the sand layer. Thin black lines represent the final bottom configurations computed by the model, thick black lines show the motionless bottom while thin grey lines show the initial random waviness. Right panels: Spectra of the final bottom configurations. The amplitude of the Fourier components is plotted versus the streamwise harmonic.

5 Discussion

The idealised process-based models described in the previous sections provide support for the experimental findings of Porcile et al. (2020). Particularly, the models reproduce the same observed effects of sediment starvation on the genesis of sand dunes in steady currents when an unerodable bottom is exposed by the growth of the bedforms. Both a stability analysis based on the numerical simulation of small amplitude perturbations of the bottom configuration and a fully numerical commercial code able to simulate the time development of finite amplitude bedforms predict the lengthening of sediment starved dunes as their growth progressively exposes the motionless substratum, with increasing irregularity of their morphology and spacing. Despite the overestimation of alluvial dune wavelength obtained by using these two different approaches, both models are able to reproduce the lengthening of the starved dunes as observed in a laboratory flume (Figure 6).

The key findings of our modelling study also agree with existing field measurements of starved fluvial dunes. Kleinhans et al. (2002) described the observations and measurements of several type of bedforms in the gravel-bed river Allier (Moulis, France) over a period of low flow during which the river bed was fully armoured. Sand wave fields of fine sand (ds $\simeq 0 \div 5$ mm), the area of

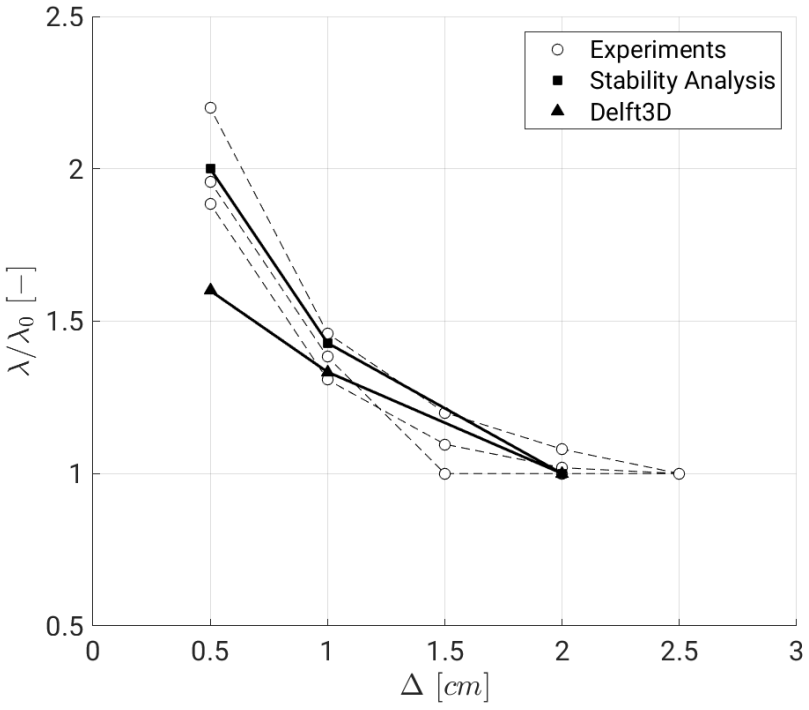

Figure 6: Comparisons of modelling outcomes with experimental measurements of the lengthening of starved dunes. Values of starved dune crest-to-crest distances are normalised by the wavelength of alluvial dunes observed for the same hydrodynamic and morphodynamic parameters and then plotted versus the thickness Δ^* of the sand layer initially available for transport.

which ranges from few squared metres to few hundreds of metres, were found to migrate over the armour layer (85% gravel, ds $\simeq$ 18 mm) as a result of bank erosion and detachment of sand from meander pools. These sand waves provided a spatially varying supply of mobile sediment for the formation of bedforms in equal hydrodynamic conditions and sediment parameters. Regularly spaced transverse dunes appeared in the inner part of these sand deposits, where the thickness of the sand coverage attains its maximum value. Then, these bedforms gradually changed in both the upstream and the downstream directions resulting into amorphous bedforms with more sinuous crests. At the front and rear edge of each sand wave field, the armour layer was fully exposed and amorphous dunes concurrently with sand ribbons were observed. Analogously to our model results, the field observations of Kleinhans et al. (2002) suggest that the main factor in determining the geometric characteristics of the emerging bedforms is the thickness of the layer of sediment available for transport. The gradual transition from regular alluvial dunes to irregular starved dunes is the same as that observed in the present study.

Similar starved patterns were observed by Carling et al. (2000b) in a supply limited reach of the river Rhine (Mainz, Germany). Carling et al. (2000b) report the presence well sorted medium sand (ds $\equiv$ 0:9 mm) in the form of different morphological patterns migrating over gravel lags mainly composed of pebbles and cobbles (ds $\simeq$ 10 mm). Two distinct populations of bedforms were identified: two-dimensional small dunes ($\lambda \simeq 1 \div 5$ m) with relatively straight crest, which were roughly transverse to the primary flow direction, and three-dimensional large dunes ($\lambda \simeq 20 \div 50$ m) with either amorphous or barchanoid planforms. Carling et al. (2000b) described in detail two large isolated dunes preceded by smaller starved dunes with crest-to-crest distance approximately equal to 2 m. These smaller dunes were found to migrate over the stoss side of the larger bedforms while decreasing in length ($\lambda \leq 1$ m). Further downstream they appear to have generally grown in dimensions ($\lambda \geq 2$ m) across the gentle stoss side of the parent dune up to the crestal region, where their transition to upper-stage plane bed was observed. Proceeding further downstream, the smaller dunes often reformed increasing in length migrating over the intervening gravel lags. All that being said, these field observations seem to indicate that sediment starvation manifests itself by forming static isolated large dunes as well as by affecting the dimensions of migrating small dunes. Particularly, the lengthening of the small dunes as they migrate from the gentle lee side of isolated barchan dunes to the gravel lags is consistent with the lengthening of the starved dunes predicted by our models.

Conversely, flume experiments designed to study the effects of sediment starvation on dune growth have led to contradictory results. The experiments of Kleinhans et al. (2002) and Venditti et al. (2019) identified a sequence of emerging bedforms in steady currents and the profile of these bedforms was observed to depend on the sediment available for transport. Differently with the experiments we used for our model validation, they provided sediment from upstream, observing the gradual growth of different kind of bedforms. As the sediment supply increased, Kleinhans et al. (2002) found a transition from sand ribbons to irregular sandy mounds and finally two-dimensional trasverse dunes. Despite a clear indication on the dimensions of starved dunes

with respect their alluvial counterparts was not provided, their findings seem qualitatively in agreement with our modelling results.

Differently, the experiments of Tuijnder et al. (2009) show dune geometries that progressively decrease in size as the availability of mobile sediment decreases and the immobile coarser underlayer is bared by the growth of the dunes. Among the several possible explanations to the contradiction between these observations and our results (see Porcile et al., 2020 for an extensive discussion), we believe the difference in the sediment and the associated skin roughness to be crucial. Tuijnder et al. (2009) employed two different grain sizes for the immobile substrate and the mobile layer. The coarser grain size of the substrate was selected to be immobile under the action of the forcing flow. As a consequence, the exposition of the substrate led not only to sediment starvation, but also to a discontinuity in skin bottom roughness. Conversely, our numerical modelling and the experiments used for its validation assume a substrate roughness which is the same as the skin roughness representing the one single grain size available for transport. Both models used in this study would require additional developments to include the effects of nonlinearities due to discontinuities in the bottom roughness.

Furthermore, a striking difference between both approaches is the predicted dune shape. It can be seen that the linearised model predicts purely sinusiodal shapes, whereas the fully nonlinear model predicts non-sinusoidal, asymmetric shapes. Comparing this bottom profile with the triangular-shaped dunes observed in the laboratory experiments, this clearly confirms the general idea that strong nonlinearities imply asymmetric dunes.

Less information is available in the literature on the effect that sediment starvation has on the migration of bedforms. The experimental measurements reproduced by our modelling results cannot reveal useful information on starved dunes migration as they were conducted without recirculation of the sediment and thus limited in time (the experiments lasted only 30 minutes. Thus, future experimental and modelling studies are required to properly investigate the effects that the lack of mobile sediment has on bedform migration. Finally, in order to place this work within a broader field of research, the (2DV) hydrodynamic model could be straightforwardly extended in the third direction. There is a body of work that shows that eolian dune size and spacing is the result of finite-amplitude interactions and how these interactions can cause the lengthing of desert barchan dunes (Hersen et al., 2004; Worman et al., 2013; Khosronejad and Sotiropoulos, 2017). However, an extension of the present modelling to account for three-dimensional effects could be used for discussing subaqueous barchan dunes as a prominent example of dunes in a sediment-limited environment, rather than necessarily reflecting only finite-amplitude interactions. Moreover, the fully nonlinear Delft3D model is currently also used to study sediment starvation in tidal sand waves (Damveld et al., 2021). Hopefully, the flow module of the model could also be extended to study the atmospheric boundary layer making the present stability analysis able to investigate the effects of sediment starvation on the morphology of eolian sandy patterns.

6 Conclusions

In this study two different process-based modelling techniques have been applied to investigate the genesis of fluvial dunes in case of sediment starvation. Previous laboratory experiments of Porcile et al. (2020) have been used to provide controlled empirical fundations for the development of process-based idealised models able to reproduce the effects that sediment starvation has on the growth of these bedforms. An hypothesis has been formulated which states that the lack of sand affects sediment transport and, in turn, bedform pattern, when a motionless substratum is exposed by the formation of fluvial dunes. This hypothesis has then been tested by means of numerical simulations in the framework of the stability analysis of a sandy bottom forced by steady currents as well as the fully numerical modelling of its time development.

Generally, the laboratory measurements indicate that the exposition of the rigid bottom strongly affects the characteristics of the emerging dunes, whose spacing increases and become more irregular with a decreasing initial sediment availability. In line with these experimental findings, simulations of the short-term time-development of small-amplitude dunes performed by means of the stability-based model predict starved dunes with longer crest-to-crest distances than those of alluvial dunes for the same values of hydrodynamic and morphodynamic parameters. Finally, similar modelling outcome has been obtained by the finite-amplitude model confirming the lengthening of starved fluvial dunes. Differently from the stability analysis, this fully numerical model is able to reproduce final bottom configurations whose profile is even closer to that observed during laboratory experiments, as it accounts for nonlinear effects other than sediment starvation. This paves the way to the modelling of field-scale starved dunes and to potentially deal with the long-term dynamics of these patterns to describe their equilibrium geometry and migration. Also, an extension of our modelling exercise would allow to include further nonlinear mechanisms that have been neglected so far, such as those associated with gravity, bottom roughness, sediment sorting and three-dimensional flow and sediment transport.

7 Data Availability Statement

Datasets for this research are included in the following paper (and its supplementary information files): Porcile, G., Blondeaux, P. and Colombini, M. 2020. Starved versus alluvial river bedforms: an experimental investigation, Earth Surface Processes and Landforms, vol. 45 (5), pp. 1229-1239, https://doi.org/10.1002/esp.4800.

References

J. Allen. The nature and origin of bed-form hierarchies. Sedimentology, 10(3):161–182, 1968.

P. Blondeaux, G. Vittori, and M. Mazzuoli. Pattern formation in a thin layer of sediment. Marine Geology, 376:39–50, 2016.

P. Carling, E. Golz, H. Orr, and A. Radecki-Pawlik. The morphodynamics of fluvial sand dunes in the River Rhine, near Mainz, Germany. I. Sedimentology and morphology. Sedimentology, 47(1):227–252, 2000a.

P. Carling, J. Williams, E. Golz, and A. Kelsey. The morphodynamics of fluvial sand dunes in the River Rhine, near Mainz, Germany. II. Hydrodynamics and sediment transport. Sedimentology, 47(1):253, 2000b.

M. Colombini. Revisiting the linear theory of sand dune formation. Journal of Fluid Mechanics, 502:1–16, 2004.

M. Colombini and A. Stocchino. Finite-amplitude river dunes. Journal of Fluid Mechanics, 611: 283–306, 2008.

M. Colombini and A. Stocchino. Ripple and dune formation in rivers. Journal of Fluid Mechanics, 673:121, 2011.

M. Colombini and A. Stocchino. Three-dimensional river bed forms. Journal of Fluid Mechanics, 695:63–80, 2012.

J. H. Damveld, B. W. Borsje, P. C. Roos, and S. J. M. H. Hulscher. Horizontal and vertical sediment sorting in tidal sand waves: Modeling the finite-amplitude stage. Journal of Geophysical Research: Earth Surface, 125(10): e2019JF005430, 2020. ISSN 2169-9003. doi: 10.1029/2019JF005430. URL https://agupubs.onlinelibrary.wiley.com/doi/abs/10.1029/2019JF005430.

J. H. Damveld, G. Porcile, P. Blondeaux, and P. C. Roos. Nonlinear dynamics of sand waves in sediment scarce environments. In EGU General Assembly 2021, 2021. doi: 10.5194/egusphere-egu21-16019.

F. Engelund. Instability of erodible beds. Journal of Fluid Mechanics, 42(2):225–244, 1970.

F. Engelund and J. Fredsoe. Sediment ripples and dunes. Annual Review of Fluid Mechanics, 14(1):13–37, 1982.

R. Fernandez Luque and R. Van Beek. Erosion and transport of bed-load sediment. Journal of hydraulic research, 14(2):127–144, 1976.

J. Fredsøe. On the development of dunes in erodible channels. Journal of Fluid Mechanics, 64 (1):1–16, 1974.

J. Fredsøe and R. Deigaard. Mechanics of coastal sediment transport, volume 3. World scientific, 1992.

H. P. Guy, D. B. Simons, and E. V. Richardson. Summary of alluvial channel data from flume experiments, 1956-61. US Government Printing Office, 1966.

P. Hersen, K. H. Andersen, H. Elbelrhiti, B. Andreotti, P. Claudin, and S. Douady. Corridors of barchan dunes: Stability and size selection. Physical Review E, 69(1):011304, 2004.

J. F. Kennedy. The formation of sediment ripples, dunes, and antidunes. Annual review of fluid mechanics, 1(1):147–168, 1969.

A. Khosronejad and F. Sotiropoulos. On the genesis and evolution of barchan dunes: morphodynamics. Journal of Fluid Mechanics, 815:117–148, 2017.

M. Kleinhans, A. Wilbers, A. De Swaaf, and J. Van Den Berg. Sediment supply-limited bedforms in sand-gravel bed rivers. Journal of sedimentary research, 72(5):629–640, 2002.

G. R. Lesser, J. A. Roelvink, J. A. T. M. van Kester, and G. S. Stelling. Development and validation of a three-dimensional morphological model. Coastal Engineering, 51(8–9):883–915, 2004. ISSN 0378-3839. doi: 10.1016/j.coastaleng.2004.07.014. URL http://www.sciencedirect.com/science/article/pii/S0378383904000870.

G. Parker, P. C. Klingeman, and D. G. McLean. Bedload and size distribution in paved gravel-bed streams. Journal of the Hydraulics Division, 108(4):544–571, 1982.

G. Porcile, P. Blondeaux, and G. Vittori. On the formation of periodic sandy mounds. Continental Shelf Research, 145:68–79, 2017.

G. Porcile, P. Blondeaux, and M. Colombini. Starved versus alluvial river bedforms: an experimental investigation. Earth Surface Processes and Landforms, 45(5):1229–1239, 2020.

A. Reynolds. A decade's investigation of the stability of erodible stream beds. Hydrology Research, 7(3):161–180, 1976.

K. J. Richards. The formation of ripples and dunes on an erodible bed. Journal of Fluid Mechanics, 99(3):597–618, 1980.

G. Seminara. Fluvial sedimentary patterns. Annual Review of Fluid Mechanics, 42:43–66, 2010.

A. P. Tuijnder, J. S. Ribberink, and S. J. Hulscher. An experimental study into the geometry of supply-limited dunes. Sedimentology, 56(6):1713–1727, 2009.

V. A. Vanoni and N. H. Brooks. Laboratory studies of the roughness and suspended load of alluvial streams. US Army Engineer Division, Missouri River, 1957.

J. G. Venditti, P. A. Nelson, R. W. Bradley, D. Haught, and A. B. Gitto. Bedforms, structures, patches, and sediment supply in gravel-bed rivers. Gravel-Bed Rivers: Process and Disasters, 439, 2017.

J. G. Venditti, J. A. Nittrouer, M. A. Allison, R. P. Humphries, and M. Church. Supply-limited bedform patterns and scaling downstream of a gravel–sand transition. Sedimentology, 66(6): 2538–2556, 2019.

684 S. L. Worman, A. B. Murray, R. Littlewood, B. Andreotti, and P. Claudin. Modeling emergent
685 large-scale structures of barchan dune fields. Geology, 41(10):1059–1062, 2013.